



OPEN ACCESS

EDITED BY

Chenxi Li,
Tianjin University, China

REVIEWED BY

Jingyuan Yang,
Peking Union Medical College Hospital
(CAMS), China
Xiao Zhang,
Peking Union Medical College Hospital
(CAMS), China

*CORRESPONDENCE

Bin Sun,
✉ sunbineye@163.com

[†]These authors have contributed equally
to this work

RECEIVED 15 June 2023

ACCEPTED 17 July 2023

PUBLISHED 27 July 2023

CITATION

Dai Y, Wang K, Zheng D, Li G, Wang K,
Wang X and Sun B (2023), Quantitative
analysis of choroidal alterations in thyroid
eye disease using swept-source OCT.
Front. Phys. 11:1240728.
doi: 10.3389/fphy.2023.1240728

COPYRIGHT

© 2023 Dai, Wang, Zheng, Li, Wang, Wang
and Sun. This is an open-access article
distributed under the terms of the
[Creative Commons Attribution License
\(CC BY\)](https://creativecommons.org/licenses/by/4.0/). The use, distribution or
reproduction in other forums is
permitted, provided the original author(s)
and the copyright owner(s) are credited
and that the original publication in this
journal is cited, in accordance with
accepted academic practice. No use,
distribution or reproduction is permitted
which does not comply with these terms.

Quantitative analysis of choroidal alterations in thyroid eye disease using swept-source OCT

Yining Dai^{1†}, Kailu Wang^{1†}, Dongping Zheng¹, Guangxu Li^{2,3},
Kang Wang², Xin Wang² and Bin Sun^{1*}

¹Shanxi Eye Hospital Affiliated with Shanxi Medical University, Taiyuan, Shanxi, China, ²School of Electronic and Information Engineering, Tiangong University, Tianjin, China, ³Tianjin Key Laboratory of Optoelectronic Detection Technology and System, Tianjin, China

Purpose: To investigate choroidal alterations in patients with thyroid eye disease (TED) using swept-source optical coherence tomography (SS-OCT) and compare them with age-matched healthy controls.

Methods: SS-OCT scans were performed to obtain quantitative measurements of choroidal parameters. Mean choroidal thickness (MCT), choroidal vessel volume (CVV), choroidal stroma volume (CSV), choroidal vascularity index (CVI), and choroidal stroma-to-vessel volume ratio (CSVR) were calculated and compared between TED and control eyes.

Results: TED eyes exhibited significantly higher MCT ($276.25 \pm 58.75 \mu\text{m}$ vs. $236.86 \pm 45.02 \mu\text{m}$, $p < 0.001$), CVV ($21.46 \pm 5.10 \text{ mm}^3$ vs. $18.14 \pm 3.83 \text{ mm}^3$, $p = 0.001$), and CSV ($13.86 \pm 2.80 \text{ mm}^3$ vs. $11.44 \pm 2.17 \text{ mm}^3$, $p < 0.001$) compared to control eyes. However, there were no significant differences in CVI (0.61 ± 0.02 vs. 0.61 ± 0.03 , $p = 0.838$) or CSVR (0.65 ± 0.05 vs. 0.64 ± 0.07 , $p = 0.345$) between the two groups.

Conclusion: SS-OCT effectively differentiated TED eyes from normal eyes based on choroidal alterations. The increased MCT, CVV, and CSV in TED suggest both dilated choroidal vasculature and expanded choroidal stroma. These findings highlight the potential of SS-OCT as an adjunctive imaging tool for the assessment of TED.

KEYWORDS

thyroid eye disease, swept-source optical coherence tomography, choroidal thickness, choroidal vessel volume, choroidal vascularity index

Introduction

Thyroid eye disease (TED), also known as Graves' orbitopathy or thyroid-associated ophthalmopathy, is an autoimmune disorder primarily observed in individuals diagnosed with Graves' hyperthyroidism [1]. TED is characterized by inflammatory changes and swelling of the extraocular muscles, accompanied by the expansion of orbital fat and connective tissue [2]. Clinical manifestations of TED commonly include upper eyelid retraction, periorbital edema, conjunctival inflammation, and proptosis [2]. Clinically, the most commonly used tool to assess TED activity and decide the treatment approach is the clinical activity score (CAS). A CAS value $\geq 3/7$ is indicative of active disease and implies suitability of the patient for treatment [3]. However, studies have shown unreliable

interobserver variability in CAS assessments, highlighting the need for seeking other objective methods for assessing TED [4].

With the development of imaging techniques, computed tomography (CT), magnetic resonance imaging (MRI), and ultrasonography (US) play a crucial role in the diagnosis and management of TED. CT and MRI have been widely used for the diagnosis of TED due to their ability for assessment of the muscle as well as orbital fat [5]. However, these imaging modalities are time-consuming and expensive, and they are not readily available for routine practice. Moreover, CT is also limited by the hazards associated with radiation. US offers fast and cost-effective evaluations without radiation risks, which could be used for assessment of extraocular muscles in TED. However, the unreliable intra- and interobserver variability limits its further clinical application in TED assessments and follow-up [6, 7].

Optical coherence tomography (OCT) is a rapid, noninvasive, and readily available imaging modality which has become a standard of care for evaluating retina disease. Recent studies have shown that OCT is an accurate method for measuring horizontal rectus tendons, which can differentiate TED from normal eyes [8]. With the advent of swept-source OCT (SS-OCT), enhanced light penetration through the retinal pigment epithelium (RPE) enables more effective visualization of the choroidal and scleral layers [9, 10]. Previous studies have demonstrated significant retrobulbar hemodynamic changes in TED [6, 11–15]. Since the choroidal vasculature handles 70% of the blood supply from the ophthalmic artery, choroidal imaging using SS-OCT may reveal distinctive characteristics in TED [16]. In this study, we employed a SS-OCT device to investigate choroidal alterations in TED and compared the findings with age-matched healthy controls.

Methods

Study design

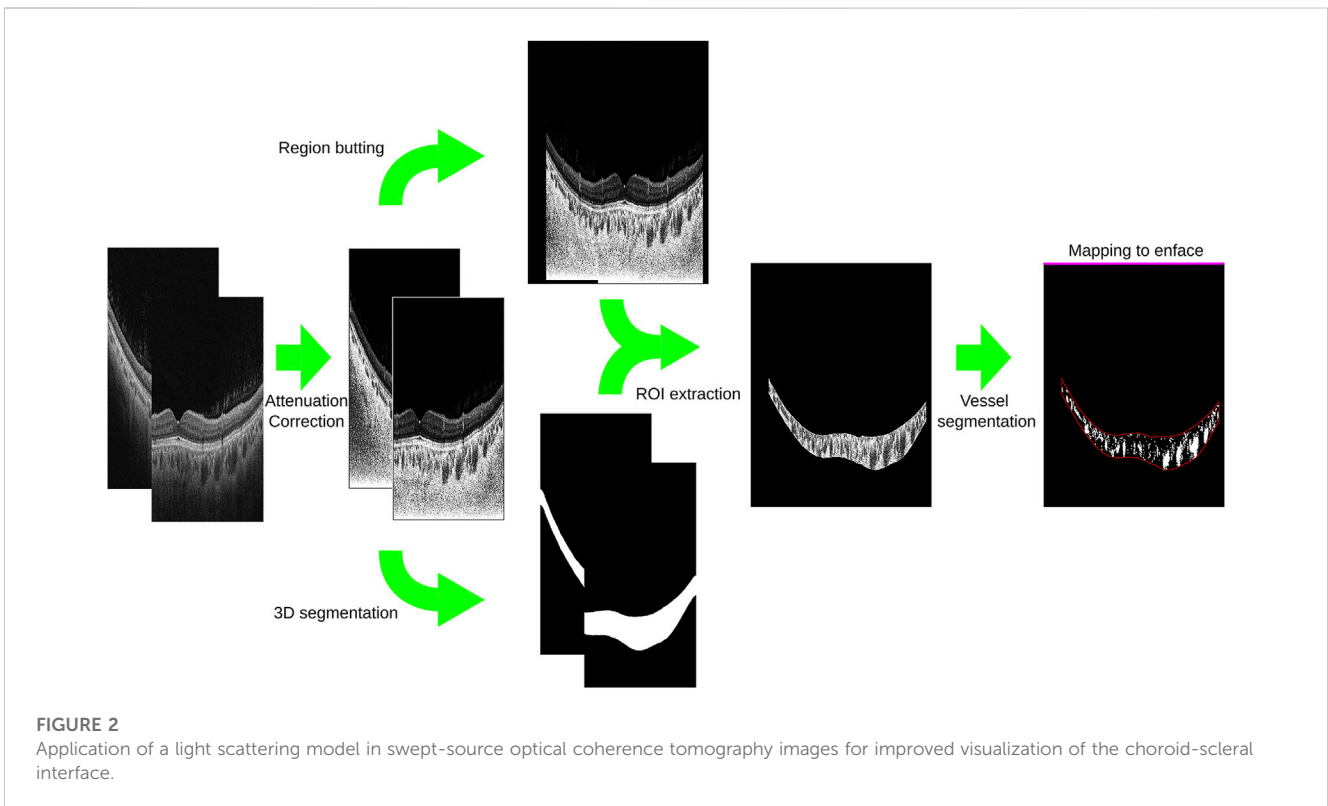
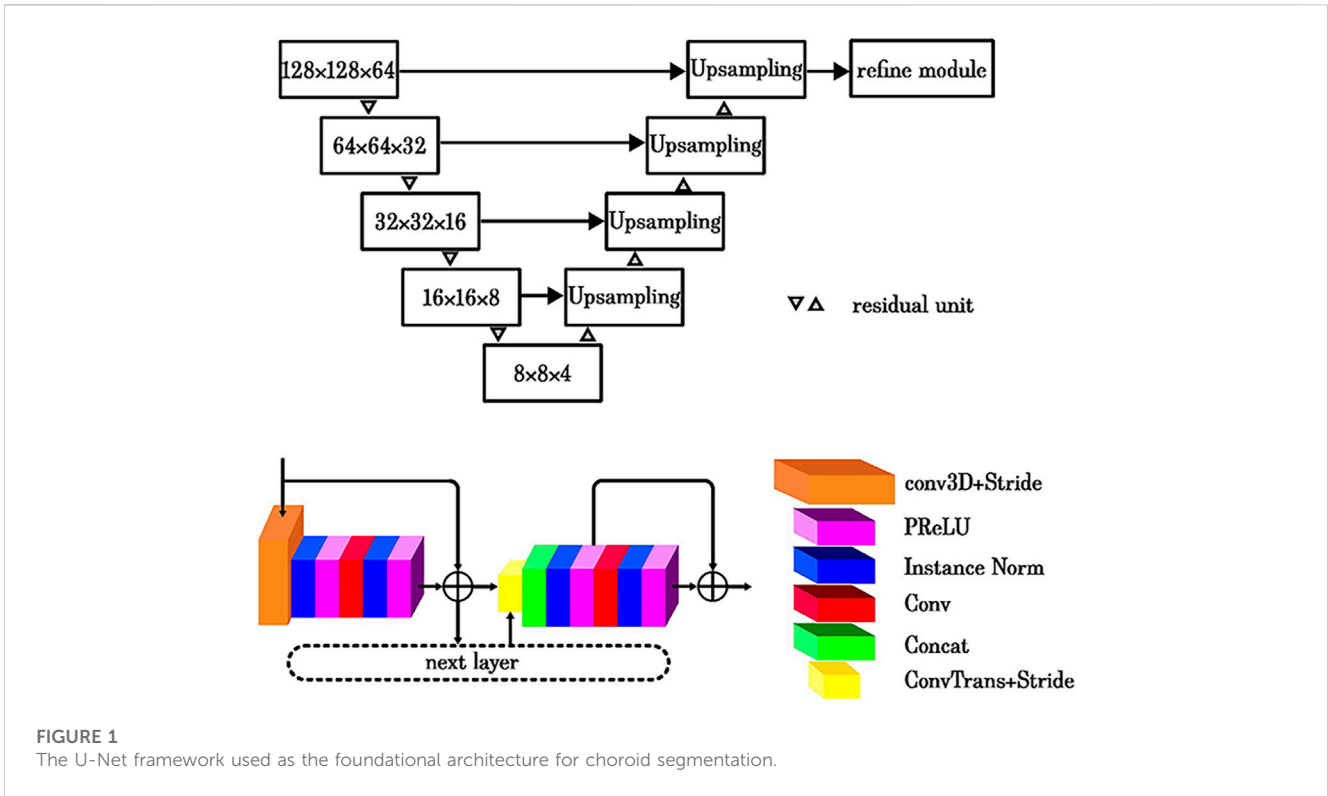
The study was started after the approval of the Institutional Review Board (IRB) of Shanxi eye hospital affiliated with Shanxi medical university. All participants provided signed IRB-approved consent prior to imaging. This prospective, comparative study was performed in adherence to the principles of the Declaration of Helsinki and in accordance with the Health Insurance Portability and Accountability Act. Patients with TED and healthy controls were recruited from Shanxi Eye Hospital between 1 April 2022, and 31 March 2023. Best corrected visual acuity was measured and recorded as the Snellen equivalent. All subjects underwent a complete ophthalmological examination. TED was diagnosed by an experienced ophthalmologist according to the criteria proposed by Bartley and Gorman [17]. Thyroid function testing, CT scans of the orbit, and Hertel's exophthalmometry were also carried out to help to confirm the diagnosis. When assessing patients for TED activity, the CAS was used [18]. Subjects were excluded if they had any ocular disease other than TED or with a history of ocular surgery. Also excluded were patients with refractive error less than -1.0 diopters or more than $+1.0$ diopters and systemic disease (such as systemic hypertension and diabetes). The right eye was selected as the study eye for each subject unless they did not meet the predefined inclusion criteria.

Image acquisition and processing

OCT scans were acquired using the PLEX Elite 9000 SS-OCT system (Carl Zeiss Meditec, Dublin, CA, USA) with a central wavelength of 1,060 nm and an acquisition speed of 100 kHz. Two 15×9 -mm² widefield OCT angiography montage scans were performed for each eye. To mitigate the influence of diurnal variation on the choroid, all acquisitions were performed between 15:00-18:00 [19]. Scans with a signal strength index below 7 or significant motion artifacts were excluded from further image processing.

The choroidal thickness map and vasculature map were generated using a previously described methodology [20]. This approach employed a U-Net framework as the foundational architecture (Figure 1) and implemented a cascaded strategy to optimize the accuracy of choroid segmentation. The first step involved addressing intensity attenuation in SS-OCT images by leveraging a light scattering model (Figure 2), which effectively reduced heterogeneity within retinal layers and enhanced the choroid-scleral interface [21]. The second component incorporated an enhanced three-dimensional (3D) U-Net model [22]. The U-Net architecture featured an encoder and a decoder with a symmetric design. The encoder utilized residual units to capture and propagate contextual information, thereby mitigating the degradation issues typically associated with deep networks. The decoder reconstructed useful image features in a coarse-to-fine manner, guided by the optimized features from the encoder. To ensure the smooth continuity of the choroidal layer boundaries, a refine module was introduced, which employed a cubic B-spline approximation and interpolation algorithm. The initial control points for the refine module were derived from the filtered boundary pixels obtained from the U-Net output. A multilevel optimization strategy was implemented to strike a balance between shape smoothness and approximation accuracy [23]. The network employed a hybrid loss function [24], which combined both Dice and CrossEntropy losses. The model was initialized using the VGG-16 pre-trained model. The third component of the system involved choroidal vessel segmentation, primarily utilizing the Otsu algorithm. Subsequently, a morphological algorithm was applied as a post-processing step to eliminate image noise, with particular emphasis on removing small, isolated regions in the choroidal stroma. To ensure the precision and reliability of the choroidal segmentation, a manual review of the choroid segmentation was conducted by an expert (KW). This meticulous manual review process served as a crucial quality control measure to validate the accuracy of the obtained choroidal measurements.

For methodological consistency, a circular region with a 12.8 mm diameter, centered at the fovea, was selected as the designated quantitative area for all measurements in this study. The exclusion of the optic nerve disc area was implemented to ensure uniformity and minimize potential confounding factors that could influence the analysis. Within this defined region, the mean choroidal thickness (MCT) was calculated as the average thickness of the choroid, providing a comprehensive evaluation of choroidal thickness within the defined quantitative area of interest. To assess the characteristics of the choroidal vasculature, the choroidal vessel volume (CVV) was determined by quantifying the total volume



occupied by the choroidal vasculature within the defined choroidal slab. Conversely, the choroidal stroma volume (CSV) was obtained by subtracting the volume of the choroidal vessels from the total

defined choroidal volume. This approach facilitated the separate assessment of the vascular and non-vascular components of the choroid within the specific quantitative area. To further analyze the

TABLE 1 Comparison of choroid parameters between TED and control eyes.

	TED	Controls	<i>p</i> -Value
MCT (μm)	276.25 \pm 58.75	236.86 \pm 45.02	<0.001^a
CVV (mm^3)	21.46 \pm 5.10	18.14 \pm 3.83	0.001^a
CSV (mm^3)	13.86 \pm 2.80	11.44 \pm 2.17	<0.001^a
CVI	0.61 \pm 0.02	0.61 \pm 0.03	0.139 ^a
CSVR	0.65 \pm 0.05	0.64 \pm 0.07	0.176 ^a

TED, thyroid eye disease; MCT, mean choroidal thickness; CVV, choroidal vessel volume; CSV, choroidal stroma volume; CVI, choroidal vascularity index; CSVR, choroidal stroma-to-vessel volume ratio.

Data are mean \pm standard deviation unless otherwise indicated.

^aBy *t*-test.

Bold values suggest statistical significance (*p*-value < 0.05).

vascular density of the choroid, the choroidal vascularity index (CVI) was calculated by dividing the CVV by the total defined choroidal volume, providing a quantitative measure of the volumetric density of the vasculature within the specific region of interest in the choroid [25]. Finally, the choroidal stroma-to-vessel volume ratio (CSVR) was determined by dividing the CSV by the CVV within the defined choroidal slab, indicating the proportion of non-vascular tissue to vascular tissue in the choroid.

Statistical analysis

Statistical analysis was conducted using IBM-SPSS software version 26.0 (IBM Corporation, Armonk, New York, NY, USA). Continuous variables were presented as mean \pm standard deviations and assessed for normality using histograms and the Shapiro-Wilk test. The Student's *t*-test was employed to compare continuous variables between the TED and control groups. A significance level of *p* < 0.05 was considered statistically significant.

Results

A total of 55 eyes from 55 patients with TED were included in the study, consisting of 18 males and 37 females. Additionally, 55 eyes from age-matched control subjects (14 males and 41 females) were also included. The mean age of the TED and control subjects was 46.40 \pm 11.28 years and 46.37 \pm 11.25 years, respectively, with no significant age difference observed between the two groups (*p* = 0.406). TED eyes exhibited a mean logarithm of the minimal angle of resolution best-corrected visual acuity of 0.004 \pm 0.081 and a mean spherical equivalent of -0.003 ± 0.054 diopters. The average intraocular pressure in TED eyes was 17.39 \pm 2.75 mmHg. The duration of TED in the patients averaged 1.99 \pm 3.00 years.

After implementing attenuation correction, a distinct choroid-scleral interface was successfully identified in all cases. Table 1 provides a comprehensive overview of the quantitative measurements of choroidal parameters in both TED and control eyes. TED eyes exhibited a significantly higher MCT compared to control eyes (276.25 \pm 58.75 μm vs. 236.86 \pm 45.02 μm ; *p* < 0.001). Moreover, TED eyes showed significantly higher mean CVV (21.46 \pm 5.10 mm^3 vs. 18.14 \pm 3.83 mm^3 ; *p* = 0.001) and mean

CSV (13.86 \pm 2.80 mm^3 vs. 11.44 \pm 2.17 mm^3 ; *p* < 0.001). However, there were no significant differences observed in the CVI (0.61 \pm 0.02 vs. 0.61 \pm 0.03; *p* = 0.139) or the CSVR (0.65 \pm 0.05 vs. 0.64 \pm 0.07; *p* = 0.176) between the two groups. Figure 3 illustrates *en face* images of choroidal vasculature, along with accompanying maps illustrating various choroidal parameters, including choroidal thickness, CVI, CVV, CSV, and CSVR.

Discussion

The present study utilized a SS-OCT device to investigate alterations in the choroidal stroma and vasculature in eyes with TED compared to healthy controls. Quantitative assessments revealed significant increases in MCT, CVV, and CSV in TED eyes. These findings suggest that SS-OCT may serve as a valuable tool for distinguishing TED from normal eyes.

Previous studies using spectral-domain OCT (SD-OCT) have reported increased choroidal thickness in patients with TED, particularly in the subfoveal region, which has been proposed as a parameter for monitoring TED activity [26–28]. However, SD-OCT's limited light penetration hampers the accurate identification of the choroid-scleral border in thick choroids [29]. In contrast, SS-OCT provides enhanced visualization of this boundary, making it a superior modality for precise choroidal thickness measurement.

In addition to improved visualization, SS-OCT offers a faster scan rate, allowing imaging of larger areas with reduced motion artifacts within a limited scanning time. Moreover, to facilitate more accurate automatic segmentation of the 3-dimensional choroidal vessel and stroma, attenuation correction was applied on B-scans to enhance the choroidal contrast [21]. By evaluating the entire 12.8-mm diameter circular region, we were able to achieve more accurate information over a wider field of view (FOV) and to eliminate the error from subjective selections of some A-lines in a few B-scans [27]. Therefore, the volume assessment over a large FOV provides much more information about choroidal alterations than previous studies. Our results showed that the MCT of the posterior region in TED eyes was significantly higher than that in normal eyes, which is in accordance with previous studies using SD-OCT and SS-OCT [28, 30].

Furthermore, we also investigated whether the thickened choroid in TED is due to dilated vasculature or expanded stroma. We calculated and compared 3-dimensional volumetric

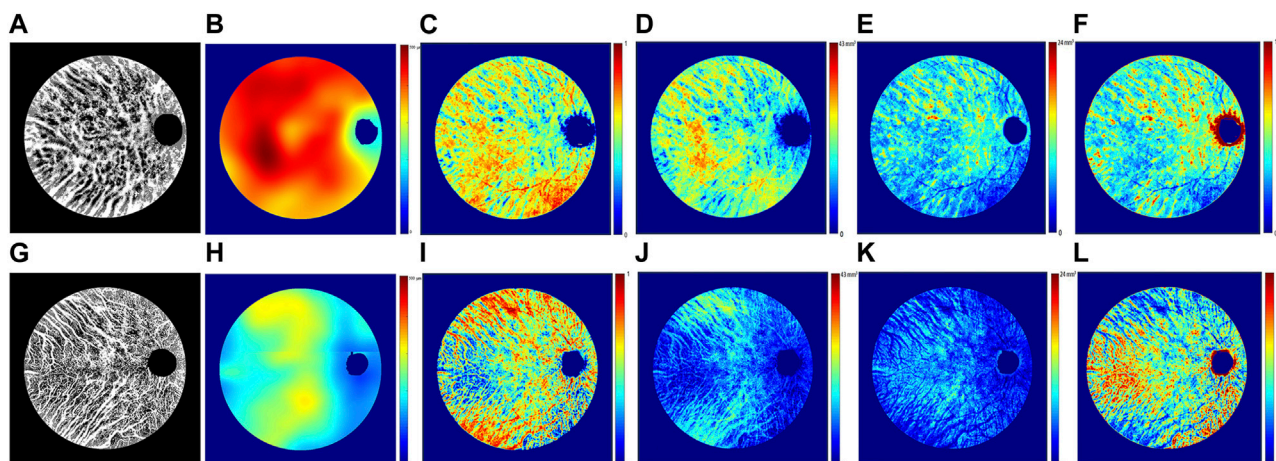


FIGURE 3

Representative *en face* images from swept-source optical coherence tomography illustrating choroidal vasculature maps (A,G), thickness maps (B,H), vascular index maps (C,I), vessel volume maps (D,J), stroma volume maps (E,K), and stroma-to-vessel volume ratio maps (F,L). Images (A–F) correspond to the right eye of a 46-year-old female patient with TED, while images (G–L) pertain to the right eye of a 47-year-old female control subject.

CVV and CSV between the two groups, which have not been reported in TED in previous studies as far as we know. Our results demonstrated significant increases in both CVV and CSV among patients with TED compared to the control group. The immune basis of TED is suggested by perivascular and diffuse infiltration of CD4⁺ and CD8⁺ T cells, B cells, plasma cells, and macrophages [31]. It has been speculated that choroidal infiltration of inflammatory cells and increased exudation may lead to an increase in choroidal thickness, resulting in the increase in CSV [26–28]. Moreover, it has been suggested that the overproduction of glycosaminoglycans by activation of choroidal fibroblasts may contribute to the increased choroidal stromal contents [32, 33]. On the other hand, in TED, the swelling of the extraocular muscles, in association with an enlargement in orbital connective tissue and fat volume, may lead to increased pressure within the orbital bony cavity [2]. Except for the compression to the optic nerve (also known as the dysthyroid optic neuropathy in severe cases), the expanded orbital tissues cause an increase in intra-orbital pressure. As a result, the venous outflow from the orbit is impeded, leading to stasis and venous dilatation of the superior orbital vein and thus increased CVV [26]. Therefore, the choroidal thickening in TED may be due to both the dilated vasculature and expanded choroidal stroma.

We also examined the volumetric density of the choroidal vasculature (CVI) and the proportion of choroidal non-vascular tissue to vasculature (CSVR) in TED. Interestingly, no significant differences in CVI or CSVR were observed between TED and normal eyes, indicating that the proportional increases in vascular and stromal components of the choroid were nearly equal, resulting in no difference in CVI or CSVR between the groups. These findings are consistent with a study by Yeter et al., which used the enhanced-depth imaging mode of SD-OCT to investigate CVI in TED [34].

Despite the enhanced capabilities of SS-OCT, it is important to recognize its limitations. One notable limitation is its inability to evaluate certain structures that undergo significant changes in TED, such as the extraocular muscle bellies and orbital fat. Additionally,

OCT still lacks the ability to distinguish between arteries and veins within the choroid. These limitations should be considered when interpreting SS-OCT findings in the context of TED assessment and understanding its full extent.

In conclusion, this study represents a novel investigation utilizing 3D volumetric choroidal measurements with SS-OCT to assess choroidal alterations in TED. The results reveal significant increases in MCT, CVV, and CSV in eyes with TED compared to normal eyes. These findings highlight the potential of SS-OCT as an adjunctive imaging tool for TED assessment. Further prospective studies with larger patient cohorts are required to validate the diagnostic capabilities of SS-OCT in TED.

Data availability statement

The raw data supporting the conclusion of this article will be made available by the authors, without undue reservation.

Ethics statement

The studies involving human participants were reviewed and approved by the Institutional Review Board (IRB) of Shanxi eye hospital affiliated with Shanxi medical university. The patients/participants provided their written informed consent to participate in this study.

Author contributions

The authors YD and BS initiated the study design. KaiW, BS, GL, KanW, and XW assisted in the collation and analysis of the data. YD, KaiW, and DZ reviewed and interpreted the data. YD drafted the manuscript, which was critically revised by all authors. Data Sharing Statement: Restrictions apply to the availability of these data, and

anonymized data will be available upon reasonable request. All authors contributed to the article and approved the submitted version.

Funding

This work was supported by the National Natural Science Foundation of China (No. 82001916), Shanxi Scholarship Council of China (No. 2022-207), Fund Program for the Scientific Activities of Selected Returned Overseas Professionals in Shanxi Province (No. 20230061), and the Open Project of Tianjin Key Laboratory of Optoelectronic Detection Technology and System (No. 2023LOTDS018).

References

- Wiersinga WM. Advances in treatment of active, moderate-to-severe Graves' ophthalmopathy. *Lancet Diabetes Endocrinol* (2017) 5(2):134–42. doi:10.1016/S2213-8587(16)30046-8
- Bahn RS. Graves' ophthalmopathy. *N Engl J Med* (2010) 362(8):726–38. doi:10.1056/NEJMra0905750
- Mourits MP, Koornneef L, Wiersinga WM, Prummel MF, Berghout A, van der Gaag R. Clinical criteria for the assessment of disease activity in Graves' ophthalmopathy: A novel approach. *Br J Ophthalmol* (1989) 73(8):639–44. doi:10.1136/bjo.73.8.639
- Perros P, Zarkovic M, Pearce SH, Razvi S, Kolli H, Dickinson AJ. Inter-observer variability of clinical activity score: Assessments in patients with thyroid eye disease. *Am J Ophthalmol* (2023) 252:94–100. doi:10.1016/j.ajo.2023.03.027
- Goncalves AC, Gebrim EM, Monteiro ML. Imaging studies for diagnosing Graves' orbitopathy and dysthyroid optic neuropathy. *Clinics (Sao Paulo)* (2012) 67(11):1327–34. doi:10.6061/clinics/2012(11)18
- Alp MN, Ozgen A, Can I, Cakar P, Gunalp I. Colour Doppler imaging of the orbital vasculature in Graves' disease with computed tomographic correlation. *Br J Ophthalmol* (2000) 84(9):1027–30. doi:10.1136/bjo.84.9.1027
- Monteiro ML, Moritz RB, Angotti Neto H, Benabou JE. Color Doppler imaging of the superior ophthalmic vein in patients with Graves' orbitopathy before and after treatment of congestive disease. *Clinics (Sao Paulo)* (2011) 66(8):1329–34. doi:10.1590/s1807-59322011000800004
- De-Pablo-Gomez-de-Liano L, Fernandez-Vigo JJ, Ventura-Abreu N, Troyano-Rivas J, Nino-Rueda C, Romo-Lopez A, et al. Optical coherence tomography thickness measurements of the extraocular rectus muscle tendons in Graves' ophthalmopathy. *J Pediatr Ophthalmol Strabismus* (2018) 55(6):356–62. doi:10.3928/01913913-20180802-01
- Fujimoto J, Swanson E. The development, commercialization, and impact of optical coherence tomography. *Invest Ophthalmol Vis Sci* (2016) 57(9):OCT1–OCT13. doi:10.1167/iov.16-19963
- Unterhuber A, Povazay B, Hermann B, Sattmann H, Chavez-Pirson A, Drexler W. *In vivo* retinal optical coherence tomography at 1040 nm - enhanced penetration into the choroid. *Opt Express* (2005) 13(9):3252–8. doi:10.1364/ope.13.003252
- Goel R, Shah S, Gupta S, Khullar T, Singh S, Chhabra M, et al. Alterations in retrobulbar haemodynamics in thyroid eye disease. *Eye (Lond)* [Ahead of print] (2023). doi:10.1038/s41433-023-02580-2
- Somer D, Ozkan SB, Ozdemir H, Atilla S, Soylev MF, Duman S. Colour Doppler imaging of superior ophthalmic vein in thyroid-associated eye disease. *Jpn J Ophthalmol* (2002) 46(3):341–5. doi:10.1016/s0021-5155(02)00485-9
- Perez-Lopez M, Sales-Sanz M, Rebollada G, Casas-Llera P, Gonzalez-Gordaliza C, Jarrin E, et al. Retrobulbar ocular blood flow changes after orbital decompression in Graves' ophthalmopathy measured by color Doppler imaging. *Invest Ophthalmol Vis Sci* (2011) 52(8):5612–7. doi:10.1167/iov.10-6907
- Tsai CC, Kau HC, Tsai HH, Kao SC, Hsu WM. Pulsatile ocular blood flow change after treatment with systemic steroid in patients with Graves' ophthalmopathy. *Eye (Lond)* (2006) 20(9):1025–9. doi:10.1038/sj.eye.6702070
- Tsai CC, Kau HC, Kao SC, Lin MW, Hsu WM, Liu JH, et al. Pulsatile ocular blood flow in patients with Graves' ophthalmopathy. *Eye (Lond)* (2005) 19(2):159–62. doi:10.1038/sj.eye.6701434
- Parver LM, Aufer C, Carpenter DO. Choroidal blood flow as a heat dissipating mechanism in the macula. *Am J Ophthalmol* (1980) 89(5):641–6. doi:10.1016/0002-9394(80)90280-9
- Bartley GB, Gorman CA. Diagnostic criteria for Graves' ophthalmopathy. *Am J Ophthalmol* (1995) 119(6):792–5. doi:10.1016/s0002-9394(14)72787-4
- Mourits MP, Prummel MF, Wiersinga WM, Koornneef L. Clinical activity score as a guide in the management of patients with Graves' ophthalmopathy. *Clin Endocrinol (Oxf)* (1997) 47(1):9–14. doi:10.1046/j.1365-2265.1997.2331047.x
- Tan CS, Ouyang Y, Ruiz H, Satta SR. Diurnal variation of choroidal thickness in normal, healthy subjects measured by spectral domain optical coherence tomography. *Invest Ophthalmol Vis Sci* (2012) 53(1):261–6. doi:10.1167/iov.11-8782
- Li G, Wang K, Wang X, Sun B, Wang K, Gao Y, et al. Volumetric choroidal segmentation using 3D residual U-Net. 9th International Conference on Computing and Artificial Intelligence (ICCAI2023) (2023).
- Zhou H, Chu Z, Zhang Q, Dai Y, Gregori G, Rosenfeld PJ, et al. Attenuation correction assisted automatic segmentation for assessing choroidal thickness and vasculature with swept-source oct. *Biomed Opt Express* (2018) 9(12):6067–80. doi:10.1364/BOE.9.006067
- Ronneberger O, Fischer P, Brox T. U-Net: Convolutional networks for biomedical image segmentation. In: *Medical image computing and computer-assisted intervention - miccai 2015; 2015 2015//*. Cham: Springer International Publishing (2015).
- Wolberg G, Lee S, Shin SY. Scattered data interpolation with multilevel B-splines. *IEEE Trans Visualization Comput Graphics* (1997) 3(3):228–44. doi:10.1109/2945.620490
- Milletari F, Navab N, Ahmadi S-A. V-Net: Fully convolutional neural networks for volumetric medical image segmentation. In: 2016 Fourth International Conference on 3D Vision (3DV); October 25–28, 2016; Stanford, CA (2016). p. 565–71.
- Yang J, Wang E, Yuan M, Chen Y. Three-dimensional choroidal vascularity index in acute central serous chorioretinopathy using swept-source optical coherence tomography. *Graefes Arch Clin Exp Ophthalmol* (2020) 258(2):241–7. doi:10.1007/s00417-019-04524-7
- Caliskan S, Acar M, Gurdal C. Choroidal thickness in patients with Graves' ophthalmopathy. *Curr Eye Res* (2017) 42(3):484–90. doi:10.1080/02713683.2016.1198488
- Yu N, Zhang Y, Kang L, Gao Y, Zhang J, Wu Y. Analysis in choroidal thickness in patients with Graves' ophthalmopathy using spectral-domain optical coherence tomography. *J Ophthalmol* (2018) 2018:1–5. doi:10.1155/2018/3529395
- Ozkan B, Kocer CA, Altintas O, Karabas L, Acar AZ, Yuksel N, et al. Choroidal changes observed with enhanced depth imaging optical coherence tomography in patients with mild Graves orbitopathy. *Eye (Lond)* (2016) 30(7):917–24. doi:10.1038/eye.2016.93
- Copete S, Flores-Moreno I, Montero JA, Duker JS, Ruiz-Moreno JM. Direct comparison of spectral-domain and swept-source oct in the measurement of choroidal thickness in normal eyes. *Br J Ophthalmol* (2014) 98(3):334–8. doi:10.1136/bjophthalmol-2013-303904
- Dave TV, Jonnadula GB, Lanka P, Natarajan R, Dave VP. Choroidal vascularity index in thyroid eye disease: Comparison with controls and application in diagnosing non-inflammatory active disease. *Orbit* (2022) 41(1):89–96. doi:10.1080/01676830.2021.2014893
- McLachlan SM, Prummel MF, Rapoport B. Cell-mediated or humoral immunity in Graves' ophthalmopathy? Profiles of T-cell cytokines amplified by polymerase chain reaction from orbital tissue. *J Clin Endocrinol Metab* (1994) 78(5):1070–4. doi:10.1210/jcem.78.5.8175962
- Maheshwari R, Weis E. Thyroid associated orbitopathy. *Indian J Ophthalmol* (2012) 60(2):87–93. doi:10.4103/0301-4738.94048
- Clark SJ, Keenan TD, Fielder HL, Collinson LJ, Holley RJ, Merry CL, et al. Mapping the differential distribution of glycosaminoglycans in the adult human retina, choroid, and sclera. *Invest Ophthalmol Vis Sci* (2011) 52(9):5511–21. doi:10.1167/iov.11-7909
- Yeter V, Kocak N, Subasi M, Parlak U. Choroidal vascularity index in thyroid-associated ophthalmopathy. *Can J Ophthalmol* (2023) 58(1):27–33. doi:10.1016/j.cjco.2021.06.023

Conflict of interest

The authors declare that the research was conducted in the absence of any commercial or financial relationships that could be construed as a potential conflict of interest.

Publisher's note

All claims expressed in this article are solely those of the authors and do not necessarily represent those of their affiliated organizations, or those of the publisher, the editors and the reviewers. Any product that may be evaluated in this article, or claim that may be made by its manufacturer, is not guaranteed or endorsed by the publisher.